Toward a Viscoelastic Modeling of Anisotropic Shrinkage in Injection Molding of Amorphous Polymers

Keehae Kwon, A. I. Isayev, K. H. Kim

Institute of Polymer Engineering, The University of Akron, Akron, Ohio 44325-0301

Received 12 August 2003; accepted 3 March 2005
DOI 10.1002/app.22399
Published online in Wiley InterScience (www.interscience.wiley.com).

ABSTRACT: A novel approach to predict anisotropic shrinkage of amorphous polymers in injection moldings was proposed using the PVT equation of state, frozen-in molecular orientation, and elastic recovery that was not frozen during the process. The anisotropic thermal expansion and compressibility affected by frozen-in molecular orientation were introduced to determine the anisotropy of the length and width shrinkages. Molecular orientation calculations were based on the frozen-in birefringence determined from frozen-in stresses by using the stress-optical rule. To model frozen-in stresses during the molding process, a nonlinear viscoelastic constitutive equation was used with the temperature- and pressure-dependent relaxation time and viscosity. Contribution of elastic recovery that was not frozen during the molding process and calculated from the constitutive equation was used to determine anisotropic shrinkage. Anisotropic shrinkages in moldings were measured at various packing pressures, packing times, melt temperatures, and injection speeds. The experimental results of frozen-in birefringence and anisotropic shrinkage were compared with the simulated data. Experimental and calculated results indicate that shrinkage is highest in the thickness direction, lowest in the width direction, and intermediate in the flow direction. © 2005 Wiley Periodicals, Inc. J Appl Polym Sci 98: 2300–2313, 2005

Key words: injection molding; orientation; polystyrene; rheology; simulations

INTRODUCTION

Shrinkage prediction for injection molded parts is influenced by the volumetric shrinkage, flow-induced residual stresses and orientation, flow-induced crystallization, and heat transfer. Since all these factors are influenced by the processing conditions, such as packing pressure, packing time, melt temperature, mold temperature, injection speed and material, and thermo-physical and rheo-optical properties, as well as geometric constraints, the prediction of shrinkage, especially of anisotropic linear shrinkage, is quite a complex issue. Clearly, the shrinkage anisotropy in moldings cannot be predicted based on volume shrinkage alone. Therefore, novel methodology for accurate prediction of development of anisotropic shrinkage of molded products is required.

For amorphous polymers, it is well known that the flow and thermal stresses become residual due to the passage through its glass transition temperature. Although the residual flow stresses are an order of magnitude smaller than the residual thermal stresses,[1] one cannot neglect the flow contribution to the overall residual stresses because the frozen-in orientation in terms of residual birefringence during molding is found to be closely related to the residual flow stresses via the stress-optical rule.

Attempts to predict frozen-in orientation in moldings of amorphous polymers were carried out by several researchers.[2–7] The empirical stress-optical rule was used to connect the residual stresses to birefringence. Isayev and Hieber[2] calculated the three frozen-in birefringence components in injection moldings during the filling and cooling stage using the Leonov constitutive equation. They approximated that the shear and normal stresses start to relax after filling of the mold due to cessation of shear flow. Flaman[3] simulated the buildup and relaxation of molecular orientation in injection-molded products and investigated the influence of the processing conditions, mold elasticity, and pressure dependence of material functions on the pressure and birefringence profiles. Recently, Isayev et al. studied the residual birefringence in molded disks[5,7] and thermal birefringence in freely quenched plates[6] of amorphous polymers. The measured birefringence data were compared with the results of numerical simulation based on the linear viscoelastic and photoviscoelastic constitutive equations.

The main origin of the anisotropy of properties in moldings is related to the orientation of molecular chains. Mechanical, optical, and other properties of polymeric products can be improved through the control of molecular orientation. The thermal expansion coefficient, compressibility, and elastic modulus of ori-

Correspondence to: A. I. Isayev (aisayev@uakron.edu).

© 2005 Wiley Periodicals, Inc.

ented polymers usually show the anisotropy closely related to orientation. Hellwege et al.[8] and Hennig[9] studied the relation between thermal expansion and draw ratio for amorphous polymers and found the linear thermal expansion along the draw direction decreases with draw ratio while that in the perpendicular direction increases. Hennig[9] also showed that the orientation similarly affects anisotropy of the linear compressibility and linear Young's modulus. Furthermore, Retting[10] studied the effect of molecular orientation on the mechanical properties and calculated its influence on the linear thermal expansion coefficients in the parallel and perpendicular directions.

A rapid, nonhomogeneous cooling of a polymeric melt through the glass transition temperature, T_g, introduces nonequilibrium volumetric changes, frozen-in orientation, and residual stresses in final products. By following the PVT diagram from the glass transition to ambient conditions, one can obtain the average value of the final product volume.[11–13] In particular, Hellmeyer and Menges[11] were the first to approach the modeling of shrinkage by the equation of state. However, their multilayer model for shrinkage during the holding pressure phase was found to be only in qualitative agreement with experimental data. Isayev and Hariharan[12] incorporated the equation of state (PVT equation) with one-dimensional cavity filling simulation to model volumetric shrinkage. They also used the first-order rate theory for volumetric changes in conjunction with solving the transient one-dimensional heat-conduction equation with a convective heat-transfer boundary condition to simulate the density variation. However, the approach to calculate shrinkage was limited because PVT diagrams are suitable to describe isotropic shrinkage only.

Recently, several new approaches were developed to predict anisotropic shrinkage.[14–21] Bushko and Stokes[14,15] used thermorheologically simple thermoviscoelastic material model to predict the part shrinkage, warpage, and build-up of residual stresses in the injection molding process. However, they neglected flow effects and assumed that in-plane shrinkages are equivalent. Jansen and Titomanlio[16–18] proposed a simple thermoelastic model taking into account thermal and pressure effect on in-plane shrinkage and Poisson's ratio on thickness shrinkage. They assumed that during solidification no relaxation and creep occurs and stresses start to build up as soon as the temperature drops below the solidification temperature. To consider shrinkage in the length and width directions, Jansen[19] set up a model that predicts variation in modulus, Poisson's ratio, coefficient of thermal expansion, and compressibility in injection molded semicrystalline products. Hieber[20] used the PVT behavior affected by crystallinity, dependent upon the thermal, pressure, and shear stress history. Based on the modified material constants, he calculated the time-dependent gapwise shrinkage of a molded specimen prior to ejection from the cavity and compared it with measured data. Recently, Kennedy and Zheng[21] used a residual strain and thermoviscoelastic stress model to calculate the shrinkage coefficient and to predict the in-plane shrinkage in the parallel and transverse to the flow direction. However, they applied a hybrid model that used measured shrinkage to improve the theoretical prediction of shrinkage and warpage.

In the present study, a new model to predict the anisotropic shrinkage of injection molded products of amorphous polymer was proposed based on the orientation function and elastic recovery determined from the nonlinear viscoelastic constitutive equation. Numerical simulation of the viscoelastic injection molding process including filling, packing, and cooling stages was carried out. As an example, the Giesekus–Leonov constitutive equation was used to calculate the flow-induced residual stresses, frozen-in orientation, and elastic recovery. The predicted anisotropic shrinkages and birefringence were compared to the experimental data measured on moldings obtained at different processing conditions.

THEORETICAL

Governing equations

The general behavior for an incompressible, nonisothermal flow is described by transport equations: mass, momentum, and energy equation. The continuity and momentum equations are given by:

$$\frac{\partial \rho}{\partial t} + \nabla \rho \nu = 0 \tag{1}$$

$$\frac{\partial \rho \nu}{\partial t} + \nu \cdot \nabla \rho \nu = -\nabla P - \nabla \cdot \tau \tag{2}$$

where ρ is density, ν is the velocity vector, P is the pressure, and τ is the stress tensor.

The Giesekus–Leonov multi-mode viscoelastic constitutive equation[2,22] is used to describe the rheological behavior of polymer melts as:

$$\overset{\nabla}{C}_k + \frac{1}{2\theta_k}\left[C_k^2 + \frac{1}{3}(II_C^k - I_C^k)C_k - I\right] = 0 \tag{3}$$

where C_k is the elastic strain tensor in the k^{th} mode, $\overset{\nabla}{C}_k$ is the Jaumann derivative of the elastic strain tensor, I is the identity tensor, and I_C^k and II_C^k are the first and the second invariant of the elastic strain tensor, C_k.

In a nonisothermal flow under consideration, the energy equation is

$$\rho C_p\left(\frac{\partial T}{\partial t} + \nu \cdot \nabla T\right) = k\nabla^2 T + \Phi \tag{4}$$

where C_p is the specific heat, k is the thermal conductivity, and Φ is the energy dissipation function for viscoelastic flow[23] as

$$\Phi = 2s\eta_0 tr(e^2) + \sum_{k=1}^{N} \frac{\eta_k}{4\theta_k^2}\left[\frac{1}{3} trC_k \cdot \{tr(C_k^{-1}) - trC_k\} + tr(C_k^2) - 3\right] \tag{5}$$

where s is the nondimensional rheological parameter between 0 to 1, e is the deformation-rate tensor, η_k and θ_k are the viscosity and relaxation time in the k^{th} mode, and η_0 is the zero-shear viscosity such as

$$\eta_0(T) = \frac{\sum_{k=1}^{N} \eta_k(T)}{1 - s} \tag{6}$$

The temperature-dependence of viscosity and relaxation time of the k^{th} mode can be expressed by the WLF type eq. (2) as

$$\eta_k(T) = \eta_k(T_r) \cdot \frac{a_T}{a_{T_r}}, \quad \theta_k(T) = \theta_k(T_r) \cdot \frac{a_T}{a_{T_r}} \tag{7}$$

where $log a_T = \left\{ \begin{array}{ll} log a_{T_g} & T \le T_g \\ \left[-\dfrac{C_1(T - T_r)}{C_2 + T - T_r}\right] & T > T_g \end{array} \right\}$ is the shift factor, T_r is the reference temperature dependent on the polymeric material, and C_1 and C_2 are constants dependent on the reference temperature.

The pressure dependence of viscosity and relaxation time can be expressed as[24]

$$\eta_k(T, P) = \eta_k(T) \cdot \exp(\beta P), \quad \theta_k(T, P) = \theta_k(T) \cdot \exp(\beta P) \tag{8}$$

where β is the pressure coefficient of viscosity.

In this research, the following assumptions are made for the simulation of the injection molding process:

a. The thin film approximation.
b. No slip condition at the wall.
c. No inertial and body force in the momentum equation.
d. Thermal conduction in the flow direction is negligible with respect to conduction in the thickness direction.
e. No fountain flow effect at the melt front.

For one-dimensional incompressible flow in Cartesian coordinates in the filling stage, eqs. (1) and (2) are expressed as:[24]

$$\frac{\partial}{\partial x}\left(S\frac{\partial P}{\partial x}\right) = 0 \tag{9}$$

where x is the flow direction and S is the fluidity expressed as

$$S = \int_0^b \frac{z^2}{\eta} dz \text{ in Cartesian coordinate} \tag{10}$$

$$S = \frac{1}{2}\int_0^r \frac{r^3}{\eta} dr \text{ in cylindrical coordinate} \tag{11}$$

where z and r are the thickness and radial directions.

In the case of simple shear flow, the elastic strain tensor has the form

$$C_k = \begin{bmatrix} C_{11,k} & C_{12,k} & 0 \\ C_{12,k} & C_{22,k} & 0 \\ 0 & 0 & 1 \end{bmatrix} \tag{12}$$

Therefore, the stress tensor can be expressed by

$$\tau(x, z, t) = 2\mu\theta_1(T)s\dot{\gamma}\begin{bmatrix} 0 & 1 & 0 \\ 1 & 0 & 0 \\ 0 & 0 & 0 \end{bmatrix} + 2\sum_{k=1}^{N} \mu_k(T)\begin{bmatrix} C_{11,k} & C_{12,k} & 0 \\ C_{12,k} & C_{22,k} & 0 \\ 0 & 0 & 1 \end{bmatrix} \tag{13}$$

where $\dot{\gamma} = -(\partial v_x/\partial z)$ is the shear rate, $\mu_k = (\eta_k/2\theta_k)$ is the modulus of the k^{th} mode, and $\mu = (\eta_0/2\theta_1)$.

The gapwise average velocity, $\bar{v}_x$, is expressed as

$$\bar{v}_x = \frac{1}{b}\int_0^b v_x \, dz \tag{14}$$

The governing equation for C_k in eq. (3) can be expressed as follows:

$$\frac{DC_{11,k}}{Dt} - 2C_{12,k}\frac{\partial v_x}{\partial z} + \frac{1}{2\theta_k}(C_{11,k}^2 + C_{12,k}^2 - 1) = 0 \tag{15}$$

$$\frac{DC_{12,k}}{Dt} - C_{22,k}\frac{\partial v_x}{\partial z} + \frac{1}{2\theta_k}(C_{11,k} + C_{22,k})C_{12,k} = 0 \tag{16}$$

$$C_{11,k}C_{22,k} - C_{12,k}^2 = 1 \tag{17}$$

where D/Dt is the material derivative operator.

The shear stress, τ_{12}, is expressed as

$$\tau_{12} = \Lambda_x z = \eta\dot{\gamma}, \quad \Lambda_x = -\frac{\partial P}{\partial x} \tag{18}$$

By integrating eq. (14) by part and eliminating $\dot{\gamma}$ with eq. (18), the average velocity, $\bar{v}_x$, is expressed as

$$\bar{v}_x = \frac{\Lambda_x}{b}\int_0^b \frac{z^2}{\eta}\,dz = \frac{\Lambda_x}{b}\,S \tag{19}$$

From eqs. (13), (14), and (19), Λ_x is given as

$$\Lambda_x = \frac{\left(2\mu s\bar{v}_x - 2\,\Sigma_{k=1}^{N}\,\mu_k\int_0^b \frac{zC_{12,k}}{\theta_1}\,dz\right)}{\int_0^b \frac{z^2}{\theta_1}\,dz} \tag{20}$$

The elastic strain tensor components at a steady state flow, C_k^{st}, are given by[2]:

$$C_{11,k}^{st} = \frac{\sqrt{2}\,X_k}{\sqrt{1+X_k}} \tag{21}$$

$$C_{12,k}^{st} = \frac{2\dot{\gamma}X_k}{1+X_k} \tag{22}$$

$$C_{22,k}^{st} = \frac{\sqrt{2}}{\sqrt{1+X_k}} \tag{23}$$

where $X_k = 1 + \sqrt{1+4(\dot{\gamma}\theta_k)^2}$.

The shear viscosity can be expressed as

$$\eta = \eta_0 s + \sum_{k=1}^{N}\frac{2\eta_k}{1+\sqrt{1+4(\dot{\gamma}\theta_k)^2}} \tag{24}$$

During the packing stage, an extra material is forced into the cavity to compensate for volume shrinkage due to solidification. The packing pressure is built up and the corresponding density is increased. To calculate pressure build-up during the packing stage and pressure decay during the cooling stage, the following equations[24] are used:

$$G(x,t)\,\frac{\partial P}{\partial t} + \frac{1}{b}\,\frac{\partial(S\Lambda_x)}{\partial x} = -F(x,t) \tag{25}$$

where

$$G(x,t) = \frac{1}{b}\left(\frac{1}{P+\bar{P}}\right)\int_0^b\left(1-\frac{\rho}{\bar{\rho}}\right)dz \tag{26}$$

$$F(x,t) = -\frac{1}{b}\int_0^b\left(1-\frac{\rho}{\bar{\rho}}\right)\frac{\partial \ln T}{\partial t}\,dz \tag{27}$$

Equations (25)–(27) are the unified formulation for the filling, packing, and cooling stages. During the filling stage, *F(x,t)* and *G(x,t)* are negligible. Therefore, eq. (25) is reduced to eq. (9). During the packing stage, *G(x,t)* is important while *F(x,t)* is negligible. During the cooling stage, both *F(x,t)* and *G(x,t)* become important.

Residual stress, orientation function, and elastic recovery

From eq. (10), the normal stress differences and shear stress are calculated by:

$$N_1(x,z,t) \equiv \tau_{xx} - \tau_{zz} = 2\sum_{k=1}^{N}\mu_k[C_{11,k}(x,z,t) - C_{22,k}(x,z,t)] \tag{28}$$

$$N_2(x,z,t) \equiv \tau_{zz} - \tau_{yy} = 2\sum_{k=1}^{N}\mu_k[C_{22,k}(x,z,t) - 1] \tag{29}$$

$$N_3(x,z,t) \equiv \tau_{xx} - \tau_{yy} = 2\sum_{k=1}^{N}\mu_k[C_{11,k}(x,z,t) - 1] \tag{30}$$

$$\tau_{12}(x,z,t) \equiv \tau_{xz} = 2\mu s\theta_1\dot{\gamma} + 2\sum_{k=1}^{N}\mu_k C_{12,k} \tag{31}$$

In general, for amorphous polymers, the total residual birefringence, Δn_a, is the sum of the flow, Δn_a^{fl}, and thermal birefringence, Δn_a^{th}.

$$\Delta n_a = \Delta n_a^{fl} + \Delta n_a^{th} \tag{32}$$

However, for simplicity here, it is assumed that the contribution of residual thermal birefringence, Δn_a^{th}, to the total residual birefringence is negligible. Although, in general, this assumption is not necessarily true but for some polymers, for example, polystyrene, such an assumption can be made. Therefore:

$$\Delta n_a \cong \Delta n_a^{fl} \tag{33}$$

The residual flow birefringence for amorphous polymers can be calculated by the stress-optical rule during the nonisothermal flow and the subsequent relaxation. The flow birefringence in the x-z plane, Δn_a^{fl}, is given by:

$$\Delta n_a^{fl} = C_\sigma(T) \cdot \Delta\sigma(x, z, t) = C_\sigma(T) \sqrt{N_1^2(x, z, t) + 4\tau_{12}^2(x, z, t)} \tag{34}$$

where $C_\sigma(T)$ is the time-dependent stress-optical coefficient as a function of temperature. The value of frozen-in normal and shear stresses are calculated as described earlier.[2,4]

Similarly, the birefringence in the z-y and x-y directions is calculated as:

$$n_{zz} - n_{yy} = C_\sigma(T) \cdot N_2$$
$$n_{xx} - n_{yy} = C_\sigma(T) \cdot N_3 \tag{35}$$

From the residual flow birefringence, one can calculate the amorphous orientation function by

$$f_{or,1} = \frac{\Delta n_a}{\Delta n_a^0}, \quad f_{or,2} = \frac{n_{zz} - n_{yy}}{\Delta n_a^0}, \quad f_{or,3} = \frac{n_{xx} - n_{yy}}{\Delta n_a^0} \tag{36}$$

where Δn_a^0 is the amorphous intrinsic birefringence. The calculations of residual stresses and birefringence are continued until the temperature at the particular position drops below the glass transition temperature, T_g.

The total strain during flow consists of the recoverable strain, γ_e, and the inelastic or plastic strain, γ_p, as:

$$\gamma_{total} = \gamma_e + \gamma_p \tag{37}$$

The magnitude of the frozen-in recoverable strain, called the elastic recovery, is total shear strain recovered after unloading the shear stress. The transient, γ_t, and the ultimate, γ_∞, elastic recovery can be expressed as[25]:

$$\gamma_t(t) = \int_0^t \dot{\gamma}_e(\xi)\, d\xi \tag{38}$$

$$\gamma_\infty = \int_0^\infty \dot{\gamma}_e(\xi)\, d\xi \tag{39}$$

The shear rate during recovery is calculated from eq. (31) by letting shear stresses to zero as

$$\dot{\gamma}_e(t) = \frac{\sum_{k=1}^N \mu_k C_{12,k}}{\mu s \theta_1} \tag{40}$$

Anisotropy of thermal expansion coefficient and compressibility

In the case of uniaxial orientation, the linear thermal expansion coefficients (LTEC) can be evaluated by knowing the orientation function. For uniaxially oriented polymers, the relation between the thermal expansion in the direction parallel, α_x, and perpendicular, α_y, to the flow and the orientation function is given as[9,26]:

$$\alpha_x = \alpha_0(1 - f_{or}), \quad \alpha_y = \alpha_0\left(1 + \frac{f_{or}}{2}\right) \tag{41}$$

The linear compressibility, β_x and β_y, can also be calculated by relations[9] similar to eq. (41):

$$\beta_x = \beta_0(1 - f_{or}), \quad \beta_y = \beta_0\left(1 + \frac{f_{or}}{2}\right) \tag{42}$$

In eqs. (41) and (42), α_o and β_o are the LTEC and linear compressibility in the isotropic state.

In the case of injection moldings, the situation is made complex since the orientation is three dimensional, being different in the length, width, and thickness directions. Under the assumption of biaxial plane orientation, from orientation functions, one can calculate the anisotropic linear thermal expansion coefficient and compressibility in the length and width directions as:

$$\alpha_x = \alpha_0(1 - f_{or,1}), \quad \alpha_y = \alpha_0(1 - f_{or,2}) \tag{43}$$

$$\beta_x = \beta_0(1 - f_{or,1}), \quad \beta_y = \beta_0(1 - f_{or,2}) \tag{44}$$

Anisotropic shrinkage in injection moldings

The prediction of volumetric shrinkage has been based on the specific volume, V, history that a polymeric melt passes through during the injection molding process. The volumetric shrinkage can be calculated as[12]:

$$S_V = \frac{\bar{V}_i - V_f}{\bar{V}_i} \tag{45}$$

where $\bar{V}_i$ is the initial specific volume of melt and V_f is the final specific volume at room temperature. Since the polymer melt undergoes severe pressure and temperature changes in a short time, the initial specific volume cannot be assumed to be as that at constant pressure and temperature conditions. Two ap-

proaches were suggested to calculate this volume, including the average specific volume until the end of the packing stage[12] and the specific volume at the end of the packing stage.[27] In the present simulation, the initial specific volume was calculated as[12]:

$$\bar{V}_i = \frac{1}{(t_p - t_f)} \int_{t_f}^{t_p} \bar{V}(t)\, dt \tag{46}$$

where t_f is the filling time, t_p is the packing time, and $\bar{V}(t)$ is the specific volume averaged in the gapwise direction at any time for the particular cross section such that

$$\bar{V}(t) = \frac{1}{b} \int_0^b V(z, t)\, dz \tag{47}$$

The specific volume for amorphous polymers can be calculated from the Spencer–Gilmore equation of state[28] as

$$V(T, P) = \frac{1}{\rho(T, P)} = \frac{1}{\bar{\rho}} + \frac{\bar{R}}{P + \bar{P}}\, T \tag{48}$$

where

$$\bar{\rho} = \bar{\rho}_l,\ \bar{R} = \bar{R}_l,\ \bar{P} = \bar{P}_l \quad \text{if } T > T_t$$

$$\bar{\rho} = \bar{\rho}_s,\ \bar{R} = \bar{R}_s,\ \bar{P} = \bar{P}_s \quad \text{if } T < T_t$$

with $T_t = b_5 + b_6 P$.

where b_5, b_6 are the parameters of the pressure-dependent transition temperature, T_t, and $\bar{\rho}_l$, $\bar{R}_l$, $\bar{P}_l$ and $\bar{\rho}_s$, $\bar{R}_s$, $\bar{P}_s$ are the material parameters that are obtained by the fitting of eq. (48) to the experimental data on the specific volume measured above and below the glass transition temperature for amorphous polymers (as shown in Figure 7).

The shrinkage changes in the injection molded products are determined by two effects: shrinkage due to cooling effect and shrinkage due to pressure effect. The cooling effect causes all layers to experience the same thermal contraction after ejection. In addition to this, each cross section solidifies under the different pressures and tends to expand proportional to that solidification pressure. Therefore, the total shrinkage can be calculated as follows[16–19]:

$$S_i = \alpha_i(T_s - T_\infty) - \beta_i \bar{P}_s, \quad i = x, y \tag{49}$$

where T_s is the solidification temperature (T_g for amorphous polymers), T_∞ is the ambient final temperature, and $\bar{P}_s$ is the average solidification pressure at each cross section, which is calculated as

$$\bar{P}_s(x) = \frac{1}{(t_{p0} - t_f)} \int_{t_f}^{t_{p0}} P(x, t)\, dt \tag{50}$$

or[18]

$$\bar{P}_s(x) = \frac{1}{b} \int_0^b P_s(x, z)\, dz \tag{51}$$

where t_{P0} is the time at which the pressure goes to zero and $P_s(x, z)$ is the pressure when the local temperature at each z reaches T_g.

However, it was found (as shown below) that this compressibility contribution to anisotropic shrinkage due to the second term in eq. (49) with the solidification pressure calculated via eqs. (50) or (51) is negligible due to the small difference in the anisotropic compressibility introduced by the low value of orientation function developed during molding. Therefore, anisotropic in-plane shrinkages are calculated based on the thermal effect only as

$$S_i = \alpha_i(T_s - T_\infty), \quad i = x, y \tag{52}$$

At the end of the packing stage, at the position where $T > T_g$, a recovery of elastic strain, introduced during flow, occurs due to abrupt pressure decay caused by release of the packing pressure. This elastic recovery contributes to the total shrinkage, causing an abrupt planar dimension change at the time of the end of packing. It can be calculated as the total elastic recovery accumulated until the end of the packing stage as

$$S_{\gamma_\infty} = \int_0^{t_p} \dot{\gamma}_e(t)\, dt \tag{53}$$

Without affecting any volumetric shrinkage, this elastic recovery can be applied to the length and width shrinkages only, due to freezing of the extensive skin layer that causes geometric constraints that prevent thickness shrinkage during the packing stage. Due to heat transfer inside the mold cavity, the wall region is already solidified, while the core region still remains in the melt state due to the slow cooling rate in this region. This solidified wall region acts as a constraint, not allowing further shrinkage in the thickness direction. Therefore, the contribution of elastic recovery that is not frozen can be applied to cause shrinkage in the length direction and simultaneously applied to cause expansion in the width direction. At this moment, the thickness shrinkage remains constant. This way, the volumetric shrinkage is preserved. The expansion caused by the pressure removal and its con-

tribution to the anisotropic shrinkage is very small due to the very small value of compressibility. Therefore, the contribution is significantly smaller than that of elastic recovery change at the end of the packing stage.

Therefore, the final length and width shrinkages are calculated by

$$S_x = \alpha_x(T_s - T_\infty) + S_{\gamma_\infty} \quad (54)$$

$$S_y = \alpha_y(T_s - T_\infty) - S_{\gamma_\infty} \quad (55)$$

Then, the shrinkage in the thickness direction can be calculated based on the volumetric shrinkage and anisotropic in-plane shrinkage as

$$S_z \cong S_v - (S_x + S_y) \quad (56)$$

EXPERIMENTAL

Materials

In this study, polystyrene, Styron 615-APR supplied by Dow Chemical Company, is used as a representative of the amorphous polymers. The rheological model parameters with three relaxation modes were obtained by curve fitting of the viscosity data, measured by Lee et al.,[29] to eqs. (7) and (24). Experimental data by Lee et al. were obtained by using two instruments: Rheometrics Mechanical Spectrometer and Instron Capillary Rheometer. This was done to cover a wide range of shear rates required for injection molding simulation. This fit and experimental data are shown in Figure 1. The specific volume data for polystyrene was obtained from Oels and Rehage[30] and fitted to the Spencer–Gilmore equation, eq. (48). This fit and experimental data are shown in Figure 2. The material parameters for PS 615 are shown in Table I.

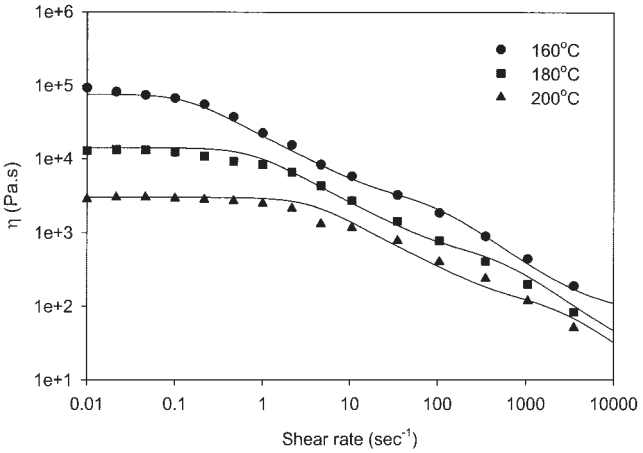

Figure 1 Flow curves at various processing temperatures as a function of shear rates for PS 615. Symbols represent the experimental data,[29] and lines indicate the nonlinear regression fit to eqs. (6), (7), and (17).

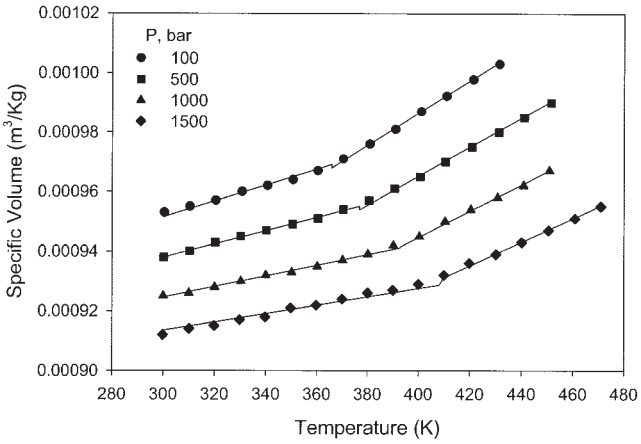

Figure 2 Specific volume versus temperature for PS 615 at different pressures. Symbols represent the experimental data,[30] and lines indicate fit by the Spencer–Gilmore equation.

Injection molding

The injection molding experiments were carried out on a Van Dorn 55F screw injection molding machine. An ASTM Charpy impact bar cavity, shown in Figure 3, was used. The injection molding experiments were carried out under different processing conditions with

TABLE I
Material and Model Parameters of PS 615

	PS	Ref.
WLF Equation:		
C_1	3.6	
C_2 (K)	131.9	[5]
T_r (K)	473.5	
Pressure-Dependent viscosity		
β (Pa^{-1})	4.3e−8	[24]
Leonov model:		
s	0.001	
T_r (K)	473.15	
η_1 (Pa · s), θ_1 (s)	2709.7, 0.1818	
η_2 (Pa · s), θ_2 (s)	186.8, 0.0107	
η_3 (Pa · s), θ_3 (s)	96.7, 3.1861e−4	
Spencer–Gilmore equation:		
$\bar{\rho}_l$, $\bar{\rho}_s$ (Kg/m^3)	1.3005e+3, 1.1480e+3	
$\bar{R}_l$, $\bar{R}_s$ (J/Kg K)	2.0445e+2, 0.4157e+2	
$\bar{P}_l$, $\bar{P}_s$ (Pa)	3.6600e+8, 1.3962e+8	
b_5 (K)	3.6236e+2	
b_6 (K/Pa)	3.0333e−7	
Δn_a^0	−0.195	[31]
C_σ (Pa^{-1})	4.8e−9	[32]
α_0 (K^{-1})	0.75e−4	[33]
β_0 (Pa^{-1})	0.0667e−9	[33]

varying packing pressure, packing time, melt temperature, and injection speed, as shown in Table II. The mold temperature of 25°C and cooling time of 30 s are used.

Anisotropic shrinkage and birefringence measurements

The shrinkage in the three different directions, that is, the length, width, and thickness directions, of injection molded samples is measured by a Digimatic caliper (Mitutoyo) for the length direction, and a Digimatic micrometer (Starett) for the width and thickness directions. The part dimensions are divided by the mold dimensions to calculate the percent shrinkage. The width and thickness dimensions are measured at three different positions along the flow direction.

To measure the birefringence distribution of injection molded PS samples, an Optical Microscope of Leitz Laborlux 12 POL S was used equipped with a 4th order compensator (Leitz Laborlux). The specimens were prepared by cutting the injection molded bars. The sample of 10 mm thickness was cut at the midway of a molded sample by using a diamond saw (Buehler Isomet). Then, the cut sample was cut parallel to the x-z plane by a diamond saw. The obtained slice of the sample has a thickness of around 300 μm. Birefringence was determined by the phase difference (retardation) between two perpendicular plane-polarized wave motions through a sample and calculated as follows:

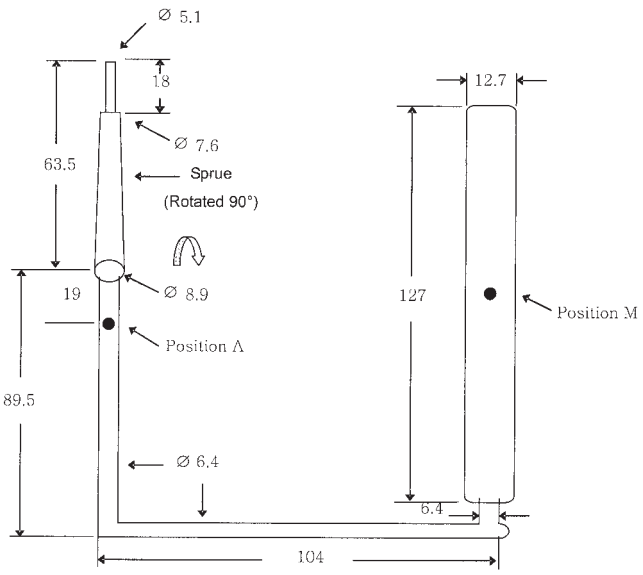

Figure 3 Dimensions of the sprue, runner, gate, and mold cavity for the ASTM impact bar mold. Cross section of the melt delivery system is circular, and that of the gate and cavity is rectangular. Thickness of cavity and gate is 3.18 mm. (All dimensions in mm).

TABLE II
Processing Conditions for Injection Molding Process

	Packing pressure (MPa)	Packing time (sec)	Flow rate (cm^3/sec)	Melt temperature (°C)
1	34.5	5	35.9	220
2	20.67	5	35.9	220
3	68.9	5	35.9	220
4	34.5	2	35.9	220
5	34.5	10	35.9	220
6	34.5	15	35.9	220
7	34.5	5	8.95	220
8	34.5	5	107.4	220
9	34.5	5	35.9	200
10	34.5	5	35.9	240

$$\Delta n = \frac{\Gamma}{d} \tag{57}$$

where Γ is the retardation and d is the sample thickness.

Meshes and numerical scheme

The numerical simulations of the injection molding process of PS were carried out by the finite difference method using ANSI C programming language. The mesh was generated over the mold cavity and the delivery system, which were divided into 12 segments and equally-spaced 182 nodes in the flow direction. The half thickness in the delivery system and the cavity was discretized by 65 nodes equally spaced.

In the filling stage, the temperature is assumed to be uniform and equal to inlet melt temperature, T_o. First, flow at the melt front was assumed to be the fully developed Poiseuille-type as the front progresses from the sprue to the end of the cavity. At the melt front nodes, $x = x_f$, the elastic strain tensor, $C_{ij,k}(x_f, z_j, t)$, can be calculated by using the steady state formulations, eqs. (21)–(23), and satisfying the shear rate and pressure gradient, eqs. (18) and (20). Then the shear rate, $\dot{\gamma}(x_f, z_j, t)$, can be obtained by solving eqs. (18) and (20)–(23) by means of the Newton–Raphson iterative method. The melt front moves along the flow direction until it reaches the end of the cavity. The elastic strain tensor, $C_{ij,k}(x_i, z_j, t)$, and shear rate, $\dot{\gamma}(x_i, z_j, t)$, at the locations other than the melt front, were determined by solving eqs. (15)–(18) and (20) by means of the Newton–Raphson iterative method. The values at the previous time are used as an initial guess for the shear rate and elastic strain tensor. After the mold cavity is filled completely, the packing stage starts.

In the packing stage, an additional melt is injected into the mold cavity to compensate the specific volume change due to cooling in this filling stage. The flow rate during the packing stage was calculated by

using the volume change between the mold cavity and the injected material at the pressure determined from eqs. (25)–(27). From the flow rate during packing, the shear rate and elastic strain tensor developed during the packing stage were obtained.

In the cooling stage, the velocity and shear rates are set to zero and the flow stresses developed during the filling and packing stages relax and are governed by the viscoelastic constitutive equation of eqs. (15)–(17). It is evident that this simulation neglects a possible backflow arising from the sudden release of the packing pressure.

RESULTS AND DISCUSSION

Simulated pressure

The calculated pressure traces obtained at two positions (see Fig. 3) in the runner (position A) and midway of the cavity (position M) are shown in Figure 4. The filling, packing, and cooling stages of pressure change can be distinguished in this Figure. The release of the packing pressure causes a fast decay of pressure in the cavity and runner.

Orientation function and anisotropic properties

Figure 5 shows the measured and calculated frozen-in birefringence at the midway of moldings obtained at different injection speeds. During the filling stage, the high shear rate near the wall lets polymer molecules be aligned along the flow direction. Therefore, the birefringence is mainly developed near the wall region due to the high shear rate and fast cooling in this region. The birefringence developed during the filling stage near the wall region gets frozen-in when melt passes through the glass transition temperature due to the fast cooling rate. In the packing stage, the birefringence starts to develop in the core region due to additional packing flow. The birefringence layer near the wall due to the flow effect is broad and low at low injection speed, while it is narrow and high at high injection speed. As the injection speed increases, the maximum birefringence near the wall increases due to enhanced flow by the high shear flow.

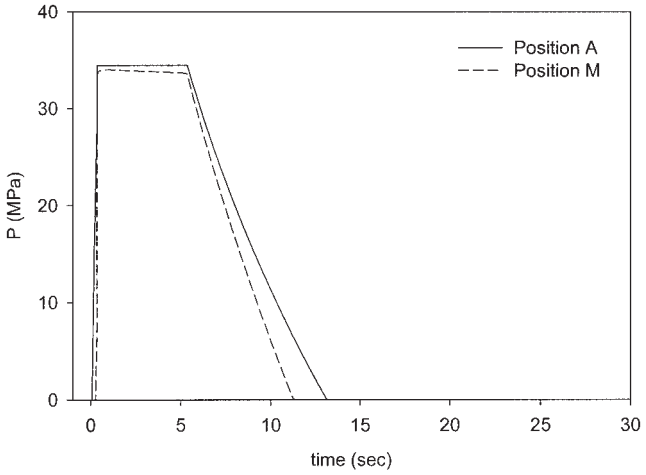

Figure 4 Calculated pressure traces in runner (position A) and midway of cavity (position M), as shown in Figure 2. Processing conditions: P_P = 34.5 MPa, t_P = 5 s, T_m = 200°C, and Q = 35.9 cm^3/s.

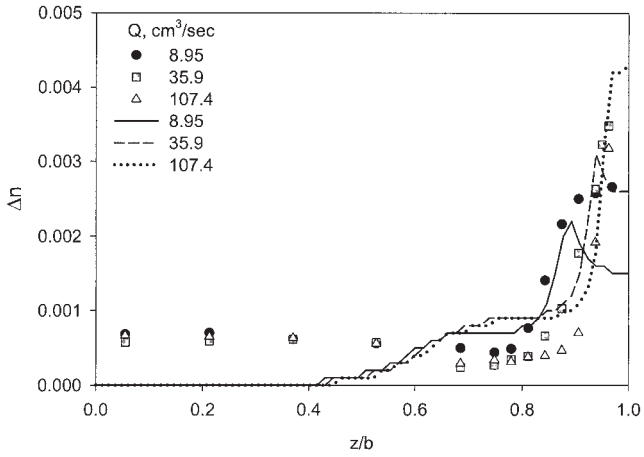

Figure 5 Gapwise distribution of measured (symbols) and calculated (lines) birefringence at midway of the cavity at various injection speeds. Processing conditions: P_P = 34.5 MPa, t_P = 5 s, and T_m = 200°C.

From the calculated birefringence, the orientation functions can be calculated. In this study, both assumptions on uniaxial and biaxial orientation are used to find the anisotropic thermal expansion and compressibility as a function of orientation. In the injection molding process, the orientation is mainly developed in the flow direction. Under the assumption of uniaxial orientation, the orientation function in the x-z direction was used. Under the assumption of biaxial orientation, orientation functions in the x-z and y-z directions were considered.

Figure 6(a) illustrates the variation of orientation function under the uniaxial orientation assumption calculated by eq. (36) at different packing times. The orientation function increases due to the increased frozen-in birefringence as the packing time increases. However, the value of the orientation function developed in amorphous polymers is very low ($\ll$1), as shown in Figure 6(a). Under the assumption of biaxial orientation, orientation functions in the length and width directions were calculated at different packing times, and results are shown in Figure 6(b). Both orientation functions increase with increasing packing time due to an increase of birefringence. However, the value of the orientation function is lower in the width direction since birefringence in that direction is low.

Figure 7 shows the calculated linear thermal expansion coefficients (LTEC) in the length and width direc-

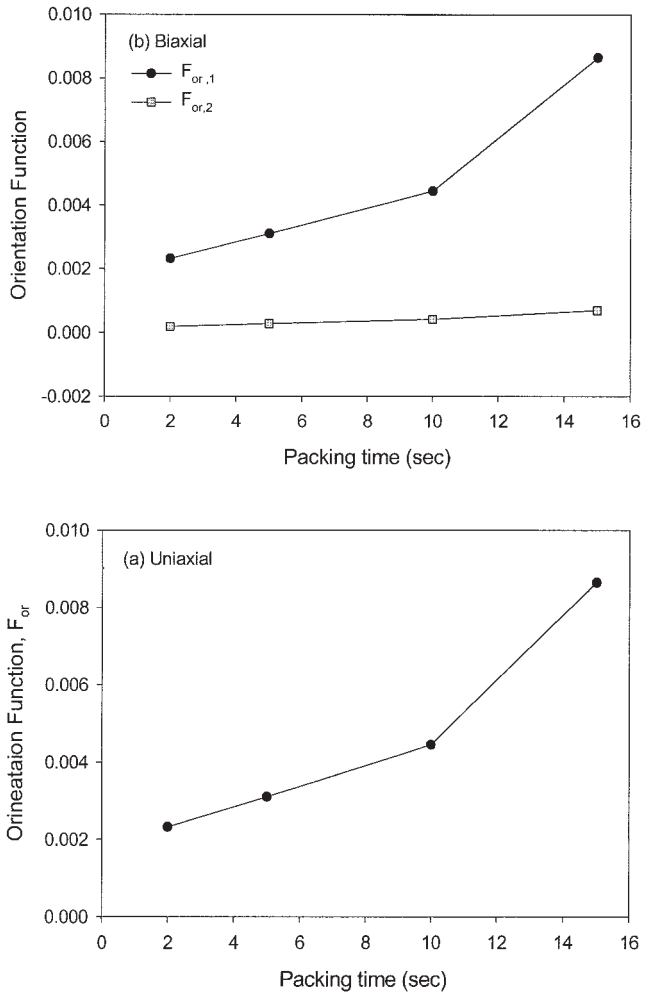

Figure 6 Predicted orientation functions as a function of packing time using the assumption of uniaxial (a) and biaxial (b) orientation. Processing conditions: P_P = 34.5 MPa, T_m = 200°C, and Q = 35.9 cm^3/s.

tions based on the orientation functions obtained at different packing times using the assumption of uniaxial and biaxial orientation, respectively. As shown in Figure 7(a), in the case of the uniaxial orientation assumption, the LTEC in the length and width directions are calculated using one orientation function and their values have different dependence on orientation. The LTEC in the flow direction decreases, while the one in the width direction increases with the orientation function, as also indicated by eq. (41). The LTEC in the flow direction is lower than in the width direction at the same amount of orientation. The linear compressibility would vary with the orientation function similarly as the LTEC, as given by eq. (42). However, in the case of the biaxial assumption, the LTEC in both the flow and width directions were calculated using two different orientation functions, but they have the same dependence on the orientation function, as indicated in Figure 7(b). The LTEC in both the flow and width directions decreases with the orientation functions, as given by eq. (43). In fact, the LTEC in the flow direction is lower than the LTEC in the width direction because of the higher orientation function in the former direction. However, it is seen from Figure 7 that the LTEC in the flow and transverse directions is not significantly different.

Also, it should be mentioned that the value of the developed orientation function in amorphous polymers in injection moldings is too small to distinguish the differences between the uniaxial and biaxial orientation assumptions.

Volumetric and anisotropic shrinkages

Using the fitted parameters shown in Table I, the variation of specific volume and resulting volumetric shrinkage were calculated during the molding process. Figure 8(a) shows the measured and calculated volumetric shrinkage in moldings as a function of

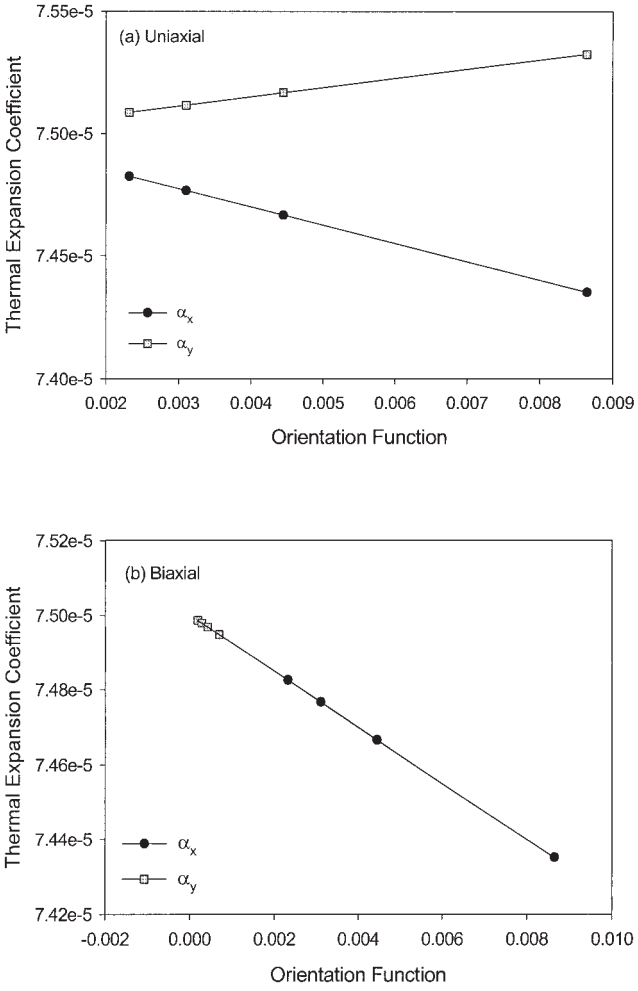

Figure 7 Predicted linear thermal expansion coefficients as a function of orientation function using the assumption of uniaxial (a) and biaxial (b) orientation obtained at different packing times. Processing conditions: P_P = 34.5 MPa, T_m = 200°C, and Q = 35.9 cm^3/s.

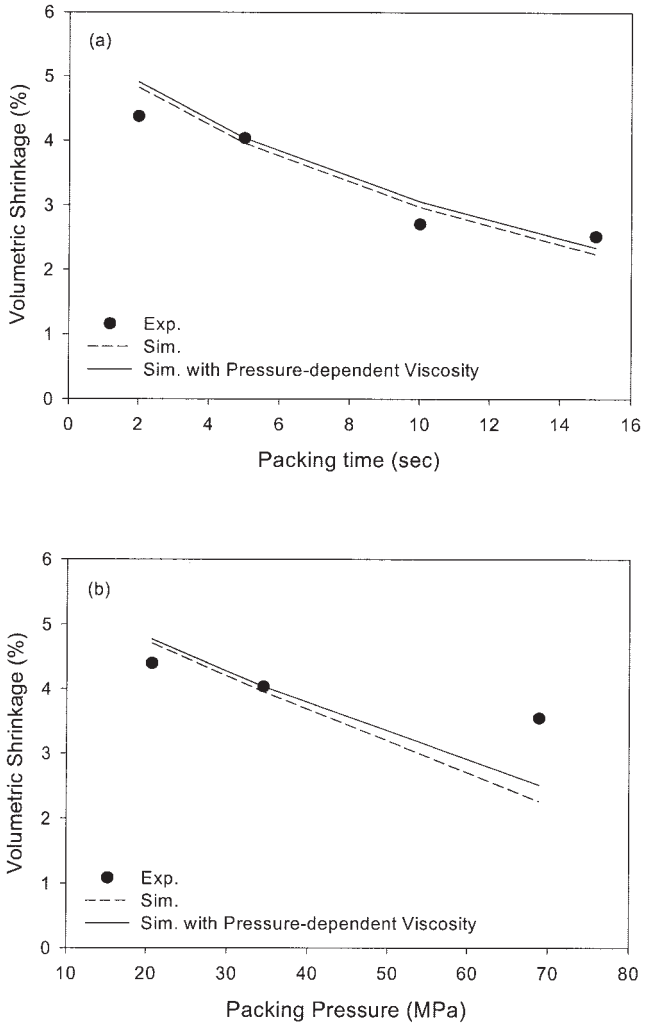

Figure 8 Measured (symbols) and predicted (lines) volumetric shrinkage with (solid line) and without (dashed line) inclusion of pressure-dependent viscosity as a function of packing time at processing conditions of P_P = 34.5 MPa, T_m = 200°C, and Q = 35.9 cm^3/s (a) and packing pressure at processing conditions of t_P = 5 s, T_m = 200°C, and Q = 35.9 cm^3/s (b).

packing times. Calculations were carried out with and without inclusion of the pressure effect on viscosity (see eq. (8)). As the packing time increases, the volumetric shrinkage decreases due to the fact that more material is injected into the cavity at longer packing times acting during the molding process. With inclusion of the pressure-dependent viscosity, the volumetric shrinkage slightly increases since the flow during the packing stage is hindered by increased viscosity. Similar to the packing time effect, the volumetric shrinkage also decreases as the packing pressure increases, as shown in Figure 8(b).

Comparisons between the measured and predicted anisotropic shrinkages are shown in Figures 9 to 12. In these Figures, the effect of processing conditions on anisotropic shrinkage, developed in molded PS strips,

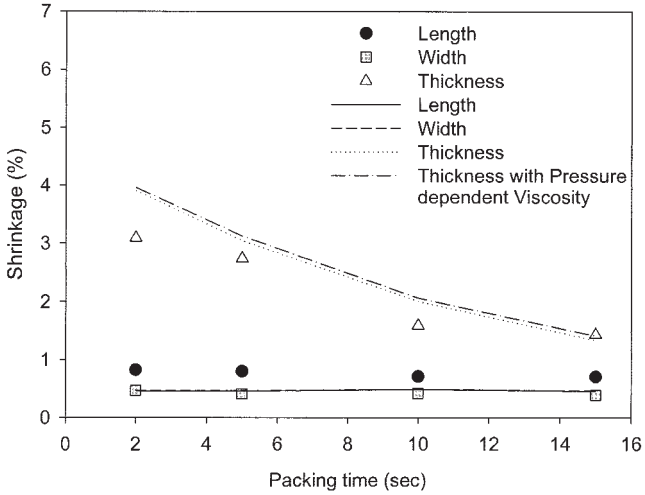

Figure 9 Measured (symbols) and predicted (lines) anisotropic shrinkages due to contributions of the thermal and compressibility effect as a function of packing time with (dotted dashed line) and without (dotted line) inclusion of pressure-dependent viscosity at processing conditions of P_P = 34.5 MPa, T_m = 200°C, and Q = 35.9 cm^3/s.

is shown. In particular, Figure 9 shows the length, width, and thickness shrinkages as a function of packing time calculated based on inclusion of both thermal and compressibility effects, as indicated by eqs. (49) and (56). Again, calculations were carried out with and without inclusion of the pressure effect on viscosity. But this effect is found to be insignificant. The anisotropic shrinkage as a function of packing time was also calculated based on inclusion of the thermal effect, but without inclusion of the compressibility

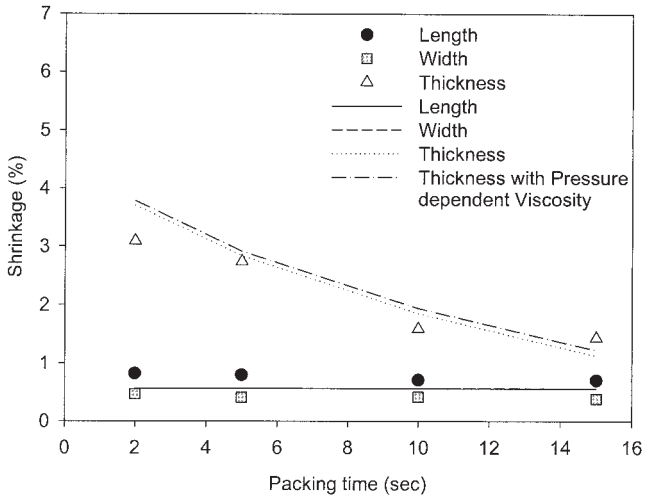

Figure 10 Measured (symbols) and predicted (lines) anisotropic shrinkages due to contribution of the thermal effect alone as a function of packing time with (dotted dashed line) and without (dotted line) inclusion of pressure-dependent viscosity at processing conditions of P_P = 34.5 MPa, T_m = 200°C, and Q = 35.9 cm^3/s.

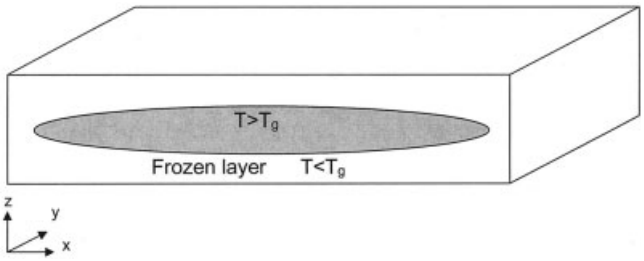

Figure 11 Schematic diagram for the frozen layer in the mold cavity.

effect, as indicated by eqs. (52) and (56). The results are shown in Figure 10. All three anisotropic shrinkages decrease with increasing packing time, with the thickness shrinkage most strongly affected by the packing time among all the shrinkages. The length and width shrinkages show a little difference with packing time since the orientation function developed in an amorphous polymer is too small, although it increases with packing time, as evident from Figure 6a. The thickness shrinkage shows the slightly better agreement with experimental data in the case of without inclusion of compressibility, as indicated by Figure 10. However, the predicted length and width shrinkage do not show any difference. They do not predict well the experimental behavior because the developed orientation is too small to affect anisotropic shrinkage.

To predict experimentally observed difference between the length and width shrinkages, the contribution of elastic recovery to the in-plane shrinkage is introduced, as given by eqs. (53)–(55). At the end of the packing time, an abrupt release of packing pressure occurs, flow ceases, and the pressure in the cavity gradually decays. At that time, an unfrozen core layer, where its temperature is above the glass transition temperature, still remains, as schematically indicated by Figure 11. As the pressure in the cavity decays, the elastic recovery in this unfrozen layer can recover very quickly and introduce a dimension change in the moldings. Due to the heat transfer inside the mold cavity and the following geometric constraint, the elastic recovery that was not frozen during the packing stage contributes to shrinkage in the length direction and expansion in the width direction. Therefore, the final anisotropic shrinkages in the length and width directions were calculated by inclusion of thermal and elastic recovery effects given in eqs. (53)–(55).

Figures 12(a) and b show the anisotropic in-plane shrinkage developed in moldings calculated by using the uniaxial and biaxial orientation assumption, respectively, along with experimental data. Due to the very small amount of orientation achieved in amorphous polymers, the calculated shrinkages based on the uniaxial and biaxial orientation do not show much difference. Therefore, further calculations in this study were conducted based on the uniaxial assumption of orientation.

Figure 13 shows the measured and calculated anisotropic shrinkages at different processing conditions. Figures 13(a,b) show the shrinkages in the three different directions of the molded parts as a function of packing time and packing pressure, respectively. As the packing time increases, shrinkage in the thickness direction decreases due to reduced volumetric shrinkage since more material is injected to compensate for the shrinkage during the packing stage. Shrinkage in the flow and width directions decreases slightly. This is due to the fact that the orientation function developed during the molding process of amorphous polymers is not high, as evident from their values depicted in Figure 5(a). Similar to the packing time effect, the thickness shrinkage decreases and the length and

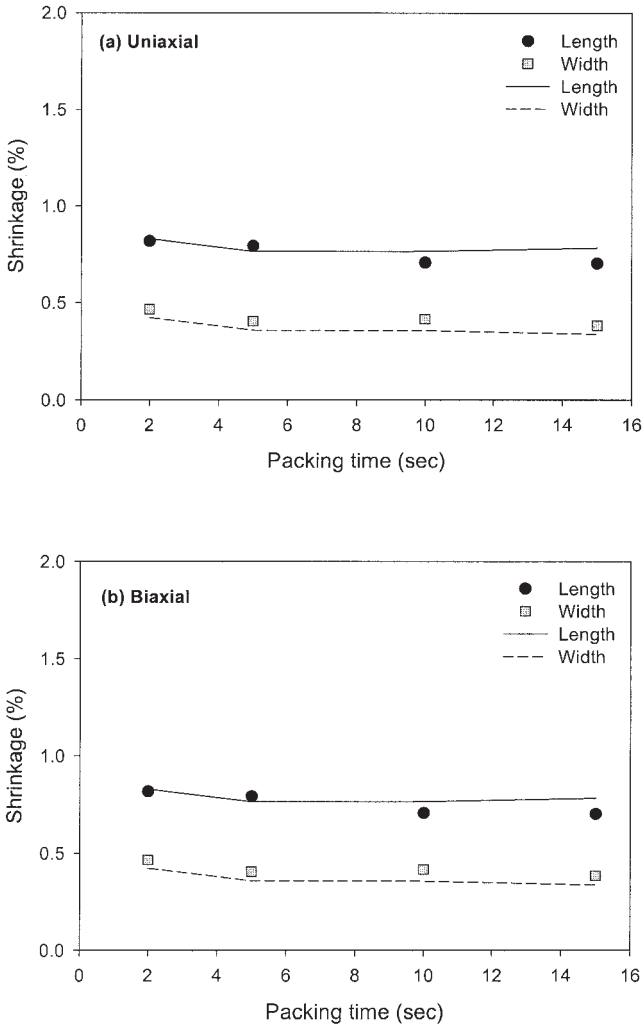

Figure 12 Measured (symbols) and predicted (lines) length and width shrinkages due to contributions of the thermal and elastic recovery effect as a function of packing time using the assumption of uniaxial orientation (a) and biaxial orientation (b). Processing conditions: P_P = 34.5 MPa, T_m = 200°C, and Q = 35.9 cm^3/s.

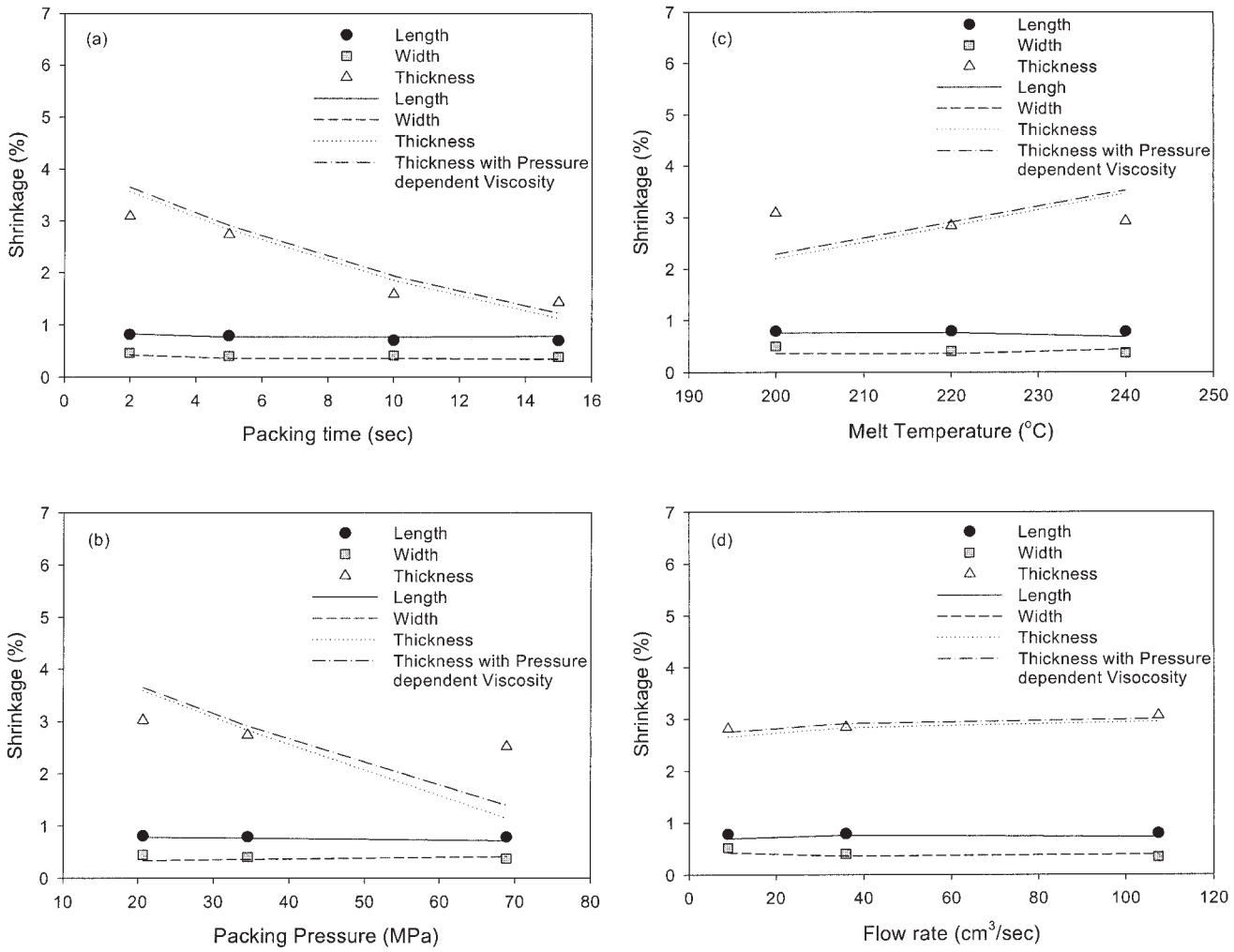

Figure 13 Measured (symbols) and predicted (lines) anisotropic shrinkage as a function of packing time (a), packing pressure (b), melt temperature (c), and injection speed (d) with (dotted dashed line) and without (dotted line) inclusion of pressure-dependent viscosity. Processing conditions: P_P = 34.5 MPa, t_P = 5 s, T_m = 200°C, and Q = 35.9 cm^3/s.

width shrinkage slightly decreases as the packing pressure increases. The thickness shrinkage is similar to that calculated based on inclusion of the thermal effect alone, as shown in Figure 10.

On the other hand, the melt temperature and injection speed have little effect on shrinkage in the length, width, and thickness directions, as noted from Figures 13(c,d). The predicted shrinkage values in the length, width, and thickness directions show a fair agreement with the experimental data. Therefore, the calculations of anisotropic shrinkages in moldings by using eqs. (53)–(56) are a suitable way to their predictions.

In many cases, it is well known that the thickness shrinkage is one order of magnitude larger than the in-plane shrinkage. In all experiments, the thickness shrinkage is always much larger than the length and width shrinkage. Also, the length shrinkage is slightly larger than the width shrinkage. In simulated results, the most important processing condition to control shrinkage and orientation is packing time and packing pressure. Especially, the thickness shrinkage is strongly affected by the packing time and packing pressure. With the variation of melt temperature and injection speed, the thickness shrinkage is only slightly affected. The length and width shrinkages are not significantly affected by processing conditions, including packing time and packing pressure. According to the comparison between experimental and simulated results, the thickness shrinkages show good agreement with experimental results. The length and width shrinkage calculated including elastic recovery contribution is also in a fair agreement with the experimental data.

CONCLUSIONS

A novel approach to predict anisotropic shrinkage in injection-molded parts of amorphous polymers was proposed based on the frozen-in orientation function

and elastic recovery. The predicted results were compared with experimental data obtained at different processing conditions, such as packing time, packing pressure, melt temperature, and injection speed. To introduce anisotropy into the shrinkage calculation, the anisotropic linear thermal expansion coefficient was calculated as a function of orientation function. The orientation function was calculated using the birefringence obtained by the stress-optical rule and the viscoelastic constitutive equation. The explicabilities of uniaxial and biaxial orientation assumptions to moldings were tested, and their effect on anisotropic in-plane shrinkage was investigated. The predicted length and width shrinkage show only a little difference due to the small amount of orientation achieved in moldings of amorphous polymers. To predict the experimentally observed difference between the length and width shrinkages, the contribution to the anisotropic shrinkage of elastic recovery that was not frozen-in during the process was considered. In agreement with experiments, the predicted thickness shrinkage was much higher than the predicted length and width shrinkages, with the length shrinkage being higher than the width shrinkage. The packing time and packing pressure were found to be the most important parameters affecting thickness and volumetric shrinkage. All predicted anisotropic shrinkages were shown to be in fair agreement with experimental results. The effects of the pressure-dependent viscosity and compressibility on anisotropic shrinkage were found to be insignificant.

This work was supported by grant DMI-0322920 from the National Science Foundation, Division of Engineering.

References

1. Isayev, A. I.; Crouthamel, D. L. Polym Plast Tech Eng 1984, 22, 177.
2. Isayev, A. I.; Hieber, C. A. Rheol Acta 1980, 19, 168.
3. Flaman, A. A. M. Polym Eng Sci 1993, 33, 193.
4. Famili, N.; Isayev, A. I. Modeling of Polymer Processing; Isayev, A. I., Ed.; Hanser Publishers: New York, 1991; Chap. 8.
5. Shyu, G. D.; Isayev, A. I. SPE ANTEC 1995, 41, 2911.
6. Shyu, G. D.; Isayev, A. I.; Li, C. T. J Polym Sci Polym Phys 2003, 41, 1850.
7. Shyu, G. D.; Isayev, A. I.; Lee, H. S. Korea-Australia Rheol J 2003, 15, 159.
8. Hellwege, K. H.; Hennig, J.; Knappe, W. Kolloid Z Z Polym 1963, 188, 121.
9. Hennig, J. J Polym Sci Part C 1967, 16, 2751.
10. Retting, W. Pure Appl Chem 1978, 50, 1725.
11. Hellmeyer, H. O.; Menges, G. SPE ANTEC 1976, 22, 386.
12. Isayev, A. I.; Hariharan, T. Polym Eng Sci 1985, 25, 271.
13. Chiang, H. H.; Himasekhar, K.; Santhanam, N.; Wang, K. K. J Eng Mater Tech, Trans ASME 1993, 115, 37.
14. Bushko, W. C.; Stokes, V. K. Polym Eng Sci 1995, 35, 351.
15. Bushko, W. C.; Stokes, V. K. Polym Eng Sci 1995, 35, 365.
16. Jansen, K. M. B.; Titomanlio, G. Polym Eng Sci 1996, 36, 2029.
17. Titomanlio, G.; Jansen, K. M. B. Polym Eng Sci 1996, 36, 2041.
18. Jansen, K. M. B.; Pantani, R.; Titomanlio, G. Polym Eng Sci 1998, 38, 254.
19. Jansen, K. M. B. Int Polym Proc 1998, 13, 309.
20. Hieber, C. A. Polym Eng Sci 2002, 42, 1387.
21. Kennedy, P.; Zheng, R. SPE ANTEC 2003, 49, 593.
22. Leonov, A. I. Rheol Acta 1976, 15, 85.
23. Sobhanie, M.; Isayev, A. I. Rubber Chem Technol 1989, 62, 939.
24. Isayev, A. I., Ed. Injection and Compression Molding Fundamentals; Marcel Dekker: New York, 1987; Chapter 1.
25. Upadhyay, R. K.; Isayev, A. I.; Shen, S. F. Rheol Acta 1981, 20, 443.
26. Choy, C. L.; Chen, F. C.; Ong, E. L. Polymer 1979, 20, 1191.
27. Han, S.; Wang, K. K. Int Polym Proc 1997, 12, 228.
28. Spencer, R. S.; Gilmore, G. D. J Appl Phys 1949, 20, 502.
29. Lee, D. J.; Isayev, A. I.; White, J. L. SPE ANTEC 1998, 44, 346.
30. Oels, H. J.; Rehage, G. Macromolecules 1977, 10, 1036.
31. Brandrup, J.; Immergut, E. H. Polymer Handbook; Wiley-Interscience: New York, 1989; 3rd ed., p 453.
32. Wales, J. L. S. The Application of Flow Birefringence to Rheological Studies of Polymer Melts; Delft University Press: The Netherlands, 1976.
33. Van Krevelen, D. W. Properties of Polymers; Elsevier: Amsterdam, 1990.